Sensors & Actuators: B. Chemical 348 (2021) 130688

Contents lists available at ScienceDirect

Sensors and Actuators: B. Chemical

journal homepage: www.elsevier.com/locate/snb

Highly sensitive non-enzymatic glucose sensor based on carbon nanotube microelectrode set

Pankaj Gupta [1], Vandna K. Gupta [2], Artur Huseinov [3], Connor E. Rahm [4], Kiera Gazica [5], Noe T. Alvarez [*,6]

Department of Chemistry, University of Cincinnati, Cincinnati, OH 45221, United States

ARTICLE INFO

Keywords:
Carbon nanotube
Copper nanoparticles
Electroanalysis
Glucose
Nonenzymatic

ABSTRACT

In this work, a carbon nanotube microelectrode set (CNT μ-ES) was modified, in which three electrodes based on highly densified carbon nanotube fiber (HD-CNT*f*) cross-sections (length ~40 μm) were embedded in an inert polymer matrix with exposed open-ended CNTs at the interface. An HD-CNT*f* cross-section (~40 μm diameter) electrochemically modified with copper nanoparticles (CuNPs) was used as the working electrode; a bare HD-CNT*f* cross-section (~94 μm diameter) was used as the counter electrode; and an HD-CNT*f* cross-section (~94 μm diameter) electroplated with Ag/AgCl and then coated with Nafion™ was used as a quasi-reference electrode. The electrochemical activity of the CuNPs/HD-CNT*f* microsensor for glucose electrooxidation was examined by cyclic voltammetry and amperometry in 0.1 M NaOH solution. As shown by amperometry studies, the proposed nonenzymatic CuNPs/HD-CNT*f* microsensor had a remarkably low limit of detection (28 nM) and a wide linear quantification range with an excellent sensitivity (1942 $nA{\cdot}\mu M^{-1}{\cdot}cm^{-2}$). This sensitivity can be attributed to the synergetic effect of electrocatalytic CuNPs and aligned HD-CNT*f*, which provide excellent conductivity. The electrooxidation of glucose on the developed microsensor was free from chloride poisoning and independent of the oxygen concentration. The developed microsensor demonstrated insignificant interference from the oxidation of common interfering species and carbohydrate compounds at their physiological concentrations. Finally, the CuNPs/ HD-CNT*f* microsensor was successfully applied for the quantification of glucose in normal human serum and diabetic patient urine samples, demonstrating the applicability of this strategy for commercial nonenzymatic glucose sensors.

1. Introduction

Glucose monitoring is of practical importance in many areas such as biotechnology, the food industry, the textile industry, and medical diagnostics. Glucose concentrations in body fluids are used as a clinical indicator of diabetes mellitus, a metabolic disorder and one of the main factors of death and disability in the world. Diabetes originates from a lack of insulin, which helps cells to adsorb glucose for energy, and results in a buildup of blood glucose levels that can damage organs including blood vessels, eyes, kidneys, and nerves [1–6]. Therefore, the rapid and accurate monitoring of blood glucose levels is required to prevent and reduce the complications of diseases associated with diabetes mellitus.

Much effort has been focused on developing inexpensive and reliable glucose sensing techniques with excellent sensitivity and selectivity, good precision, and fast response times [6,7]. In this context, various approaches including colorimetry [8], chemiluminescence [9], fluorescence [10,11], surface-enhanced Raman scattering [12,13], mass spectrometry [14,15], and electrochemical methods [6,7] have been intensely explored. Among the reported techniques, the electrochemical

* Corresponding author.
E-mail address: alvarene@ucmail.uc.edu (N.T. Alvarez).
[1] 0000-0001-7689-4352
[2] 0000-0001-9752-7818
[3] 0000-0002-4379-7668
[4] 0000-0003-0250-9946
[5] 0000-0002-4516-1233
[6] 0000-0002-8392-1483

https://doi.org/10.1016/j.snb.2021.130688
Received 29 June 2021; Received in revised form 5 August 2021; Accepted 29 August 2021
Available online 31 August 2021

detection of glucose is considered the most convenient and promising method due to its excellent selectivity and sensitivity, reliability, easy operability, low cost, long-term stability, fast detection speed, and continuous monitoring ability. Therefore, the development of electrochemical glucose sensors has received extensive interest over the past few decades [6,16,17]. The use of glucose oxidase (GOx), an enzyme that catalyzes the oxidation of glucose to gluconolactone, in the electrochemical sensing of glucose has been widely explored to achieve high sensitivity and selectivity; however, enzymatic glucose biosensors suffer from poor stability, oxygen interference, complicated immobilization procedures, and critical operating conditions. In particular, as the catalytic activity of GOx is susceptible to environmental conditions such as pH, temperature, humidity, and intrusive chemicals, reproducibility is an important issue for quality control [7,18,19]. To avoid the issue of enzyme degradation, enzyme-free glucose sensors have been explored. In recent years, attempts have been made to develop nonenzymatic glucose sensors by immobilizing various noble metal nanoparticles, including platinum [20,21], gold [22–24], palladium [25–27], and their alloys [19,28–32] on working electrode surfaces. However, reported noble-metal-modified electrodes suffer from low sensitivity and specificity due to surface poisoning by chloride ions or the adsorption of intermediate species. Moreover, because of their high cost, noble metals are not suitable candidates for the mass production of disposable nonenzymatic electrodes [6,7,19].

Copper is a widely investigated metal catalyst and is of particular interest for the fabrication of nonenzymatic glucose sensors owing to its minimal cost, outstanding electrocatalytic activity, high electrical conductivity, chloride poisoning resistance, and ready availability [33–37]. Due to the ability of copper to change valence states, copper-based materials with a variety of dimensionalities and nano/microstructures such as metallic copper [36,38–41], Cu_xO [42–44], $Cu(OH)_2$ [45–47], and Cu_xS [48–50] have been used to fabricate enzyme-free sensing interfaces to catalyze glucose electrooxidation. Furthermore, to enhance sensor performance for glucose detection, carbon nanotubes (CNTs) have been exploited as conductive templates to support copper or copper oxide nanomaterials, which greatly improves the dispersion and loading amount of metal catalysts on electrode surfaces. For instance, Male et al. fabricated a copper nanoparticles (CuNPs)/CNT-deposited glassy carbon electrode (GCE) for nonenzymatic glucose detection, which showed a four-fold increase in sensitivity compared with a bare copper disk electrode [51]. Other reported glucose sensors based on CuNPs/CNTs [2,52–55] also exhibited high sensitivity for the electrocatalytic oxidation of glucose, which was attributed to the introduction of CNTs. These studies used sonicated or randomly arranged CNTs coupled with a copper metal catalyst for glucose electrocatalytic oxidation. However, the best way to take advantage of the anisotropic properties of individual CNTs is to align them in a fiber. Aligned and highly densified CNT fibers are less influenced by solution resistance and have high mass sensitivity, electrical conductivity, and signal-to-noise ratios, which reduce the background charging current and result in lower detection limits as compared to randomly arranged or dispersed CNT electrodes [56–61]. Attempts have been made to fabricate nonenzymatic glucose sensors by depositing a copper metal catalyst using either electrochemical or sputtering methods on vertically aligned or as-grown CNTs produced by chemical vapor deposition (CVD) [62–65]. The copper-deposited CNT forests connected to a conductive support, i.e., a GCE [62,63] or a copper electrode [65] exhibited high sensitivity toward glucose electrooxidation. However, the preparation of these macrosized sensors required expensive and complicated fabrication processes, which are not suitable for mass production. Therefore, there is a strong need to explore nano-/microsized CNT arrays for the fabrication of inexpensive high-performance miniature or point-of-care sensing devices for glucose monitoring.

Thus, our goal was to fabricate a miniature glucose sensing device with the working electrode (WE), counter electrode (CE), and reference electrode all based on CNTs and assembled on a single platform that can detect an analyte in a single droplet of solution. Herein, we report the first nonenzymatic glucose sensor based on carbon nanotube microelectrode set (CNT μ-ES), in which all three electrodes are made of a highly densified, well-aligned multiwalled carbon nanotube fiber (HD-CNT*f*). The HD-CNT*f* embedded in an inert polymer film was sectioned into micrometer-length rods to obtain open-ended HD-CNT*f*. As a result, the sidewalls of the CNTs were encapsulated with only the open ends of the CNTs exposed at the interface, allowing the unparalleled sensitivity of the open ends to be exploited. As the WE, a CNT*f* cross-section electrochemically modified with CuNPs was used as the electrocatalyst for glucose oxidation. Furthermore, a Ag/AgCl/Nafion™-coated CNT*f* cross-section and a bare CNT*f* cross-section was used as the quasi-reference electrode (QRE) and the CE, respectively. Owing to the micrometer scale of these CNT*f* electrodes, the entire sensor could be miniaturized onto a single platform. The novelty of this technology lies in the μ-ES detection capabilities, where all three CNT*f* electrodes were individually connected to metallic wire leads for electronic circuit communication on one side with the modified HD-CNT*f* open ends on other side for glucose sensing. Owing to the excellent conductivity of the densely packed edge plane sites of the CNT cross-section and the outstanding catalytic ability of the CuNPs, the developed microsensor exhibited a wide linear range for glucose detection with a very low limit of detection (LOD). Notably, the glucose sensing performance of the CuNPs/HD-CNT*f* microsensor was not affected by chloride poisoning or oxygen interference. Importantly, the developed microsensor provided satisfactory results for glucose detection in diabetic patient urine samples and normal human serum, demonstrating its applicability as a practical glucose sensor.

2. Experimental section

2.1. Reagents and materials

Copper sulfate pentahydrate ($CuSO_4.5H_2O$), sulfuric acid (H_2SO_4), sodium hydroxide (NaOH), boric acid (H_3BO_3), Glucose, lactose, sucrose, fructose, ascorbic acid, dopamine, uric acid, NaCl, human serum (S1–100 mL) and urine were purchased from Sigma Aldrich. NaOH solution of 0.1 M were used as supporting electrolyte. The urine samples of diabetic patient were collected in sterile cups and used as received without any filtration or purification. Institutional Review Board (IRB) protocol was followed during human urine sample collection. For the fabrication of CNT rods embedded polymer films, EMBed-812 embedding kit consisting of monomers and cross linkers were purchased from Electron Microscopy Sciences (PA, USA) and prepared according to given instructions. CNT fiber was densified in acetone solvent for 96 h at 30 ℃ in an oven. CNT fiber was produced from CVD grown vertically aligned CNT forests as reported by our group [66,67] before where ethylene (Wright Brothers, USA) was used as the carbon source and Fe/Co as the catalyst (Goodfellow, USA). All other chemicals and solvents used in the study were of analytical grade, and Milli-Q ultrapure deionized water (18 MΩ cm) was used to prepare all the solutions.

2.2. Instrumentations

Cyclic voltammetry was performed with a computerized Bioanalytical system Epsilon EClipse™ and amperometry experiments were recorded using CHI 760E electrochemical workstation from CH instruments. The μ-ES consists of three HD-CNT*f* rods of different diameter where ~40 μm diameter coated with CuNPs was used as the working electrode (WE), ~94 μm diameter HD-CNT*f* rod coated with Ag/AgCl/Nafion™ used as quasi-reference electrode (QRE) and ~94 μm diameter bare HD-CNT*f* rod was used as counter electrode (CE). For comparison of QRE, an Ag/AgCl (3 M NaCl) (ALS Co., Ltd, Model 012167 RE-1B) was used as a standard reference electrode. Gamry Reference 600 potentiostat was used to record electrochemical impedance spectroscopy (EIS) data. Surface characterization of CuNPs/μ-ES were performed using

field emission-scanning electron microscopy (FE-SEM) FEI XL30 operated at 10 kV acceleration voltage and Raman spectra were collected using a Renishaw inVia Raman microscope, excited by a 633 nm Ar-ion laser, Gloucestershire UK. Raman spectra are collected at 5 points for each sample using ~ 10 s acquisition time with 10% power. The time and power are kept constant during Raman studies.

2.3. CNT production and microsensor fabrication

CNT fibers with different diameters were produced from vertically aligned CNT forest arrays synthesized by CVD, as reported earlier [66,67]. The vertically aligned CNT forest array was drawn from one end and twisted into a fiber using a spinning and pulling motor simultaneously. The produced fiber was held together by van der Waals attraction and the packing density of CNTs within the fiber was poor. To increase the packing density, the fiber was soaked in acetone under optimized conditions (96 h at 30 °C in an oven). The densification process improved the alignment of the CNTs within the fiber and has also been shown to increase the conductivity of CNT*f* [66,68]. Field emission scanning electron microscopy (FE-SEM) images of the acetone-soaked HD-CNT*f* with different diameters (~40 and 94 μm) are shown in Fig. 1A and B. A schematic of the fabrication process for the μ-ES using HD-CNT*f* is shown in Fig. S1 (Supporting Information, page S2). The mechanical process used to fabricate the μ-ES using HD-CNT*f* is similar to that reported in our recent studies [69,70]. Briefly, one 40 μm and two 94 μm diameter HD-CNT*f* of 1.5 cm in length were placed parallel to each other, with a spacing of 2 mm, on a tape scaffold. The HD-CNT*f* attached to the scaffold was placed vertically in a 2 mL capsule-shaped plastic vial, which was then filled with an Embed-812 monomer mixture and cured at 90 °C in an oven for 24 h. The HD-CNT*f*-embedded cured polymer capsule was removed from the plastic vial and microtomed perpendicular to the embedded CNT*f* into 40 μm thick slices, which resulted in the open ends of 40 μm long HD-CNT*f* being exposed at both sides of the sliced film. Fig. 1C displays a higher magnification image of the bare HD-CNT*f* cross-section, confirming the high-density packing of CNTs within the fiber. The exposed open ends of each HD-CNT*f* (one 40 μm and two 94 μm in diameter) on one side (electrical contact side) of the sliced film were connected to a conductive metal wire using silver paste and then encapsulated with epoxy resin for electrical insulation. The other side of the film was used as a μ-ES with the ~40 μm diameter HD-CNT*f* as the WE and the ~94 μm diameter HD-CNT*f* as the reference electrode and CE. For glucose determination, the bare HD-CNT*f* cross-section was used as the CE, whereas the reference electrode was modified with Ag/AgCl and then coated with Nafion™ to produce a QRE. Furthermore, for the WE, the 40 μm HD-CNT*f* cross-section was modified with CuNPs. The FE-SEM image of the CuNPs-based CNT μ-ES (Fig. 1D) shows the incorporation of the CuNP-modified WE, Ag/AgCl/Nafion™-modified QRE, and bare HD-CNT*f* CE (red circles).

2.4. Fabrication of Ag/AgCl//Nafion^{TM}/HD-CNTf rod QRE

For the fabrication of QRE, first Ag nanoparticles (NPs) were electroplated onto the cross section of one ~94 μm HD-CNT*f* rod using optimized 30 mM $AgNO_3$ in 1 M NH_3 solution with the help of a porous junction Ag/AgCl (3 M NaCl) and platinum wire as reference and counter electrode, respectively. The electrochemical deposition was carried out by applying an optimized reduction potential at −300 mV for 30 s in stirred $AgNO_3$ solution, and then rinsed with DI water and dried under ambient room temperature. To form a thin layer of AgCl, a drop of 50 mM $FeCl_3$ solution was casted onto the surface of AgNPs coated HD-CNT*f* cross section for 90 s and further rinsed with DI water and dried under ambient room temperature. The FE-SEM images of AgNPs/HD-CNT*f* rod and Ag/AgCl/ HD-CNT*f* rod are shown in Fig. 1E and F. The deposition of AgNPs and formation of AgCl layer was also confirmed by EDAX as shown in the Fig. S2A and B (Supporting Information), respectively. The direct exposure of Ag/AgCl/HD-CNT*f* to electrolyte solution was found to alter the potential of QRE due to possible degradation of Ag/AgCl layer in long term electrochemical calibration studies. Therefore, to avoid the alteration or degradation of the Ag/AgCl layer, a drop of 5% Nafion™ solution was casted onto the Ag/AgCl coated HD-CNT*f* rod surface (Fig. 1G). The Nafion™ coated surface was dried under ambient room temperature for 12 h and then cured in an oven at 90 °C for 1 h. The Nafion™ coating was found to provide a stable potential and maintains the integrity of the Ag/AgCl surface for extensive electrochemical testing for several days [71]. The EDAX data of Ag/AgCl/Nafion™ QRE is shown in Fig. S2C (Supporting Information).

2.5. Fabrication of CuNPs/HD-CNTf rod WE

To modify the ~40 μm diameter HD-CNT*f* rod cross section with CuNPs, the controlled potential electrolysis (CPE) was performed in an optimized 1:0.5:0.5 solution mixture of 10 mM copper sulfate solution, 0.5 mM of boric acid and 0.5 mM of sulfuric acid, respectively. Initially to optimize the CuNPs deposition on HD-CNT*f* surface different constant potential i.e., −150 mV, −250 mV, −350 mV and −450 mV were applied for 180 s (optimized). After CuNPs deposition, electrodes were rinsed with DI water and dried under ambient room temperature. The FE-SEM images of CuNPs/HD-CNT*f* fabricated at different potentials are presented in Fig. S3 (Supporting Information). The electrode prepared at −350 mV showed highest peak current for glucose electrooxidation compared to the other fabricated electrodes, therefore, an optimized −350 mV potential was selected to study the glucose electrooxidation at CuNPs/HD-CNT*f*. The micrograph of the resulting surface CuNPs/HD-CNT*f* rod is shown in Fig. 1H. The EDAX characterization of the CuNPs modified HD-CNT*f* cross section confirmed the electrochemical deposition of CuNPs on the open-ended or defective sites (sp^3 carbon) of the CNTs. The EDAX details are shown in the Fig. S4 (Supporting Information).

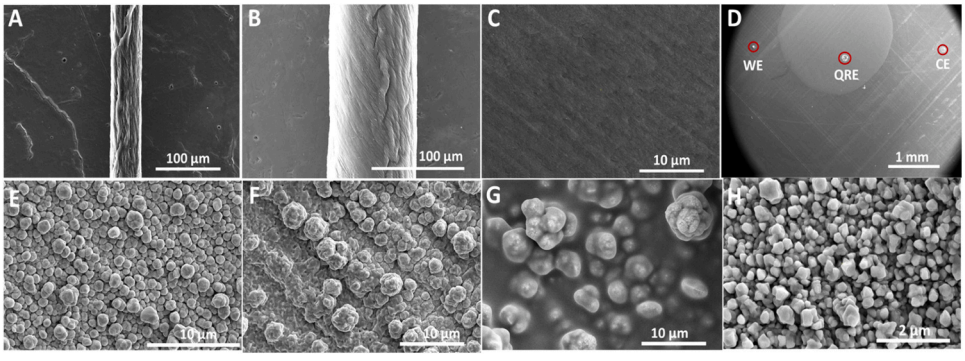

Fig. 1. FE-SEM images of (A) ~40 μm and (B) ~94 μm HD-CNT*f*; (C) high-magnification FE-SEM image of WE HD-CNT*f* cross-section, which confirms the dense packing of CNTs within the fiber; (D) polymer-embedded HD-CNT*f* cross-sections (red circles) used as the WE, QRE, and CE; (E) AgNPs electroplated on a HD-CNT*f* cross-section (~94 μm); (F) Ag/AgCl layer formed by drop-casting $FeCl_3$ on AgNPs; and (G) 5% Nafion™ coating on Ag/AgCl-modified HD-CNT*f* cross-section (QRE); (H) WE consisting of a CuNP-modified HD-CNT*f* cross-section (~40 μm). (For interpretation of the references to color in this figure legend, the reader is referred to the web version of this article.)

2.6. Experimental procedure

The 0.1 M NaOH solution was used as supporting electrolyte in all electrochemical studies. The stock solutions of glucose were prepared in deionized (DI) water. The CV measurements were performed in the potential window of −200 mV to +500 mV for calibration and scan rate studies. Amperometric measurements were recorded at optimal +400 mV potential by consecutive addition of glucose concentrations at 40 s interval time, with the current response being stable, into the stirred 0.1 M NaOH solution. The CuNPs/μ-ES was applied in triplicate ($n = 3$) for each electrochemical determination. Amperometric experiments were repeated at three electrodes for the calibration study and real samples assays. All experiments were carried out at room temperature. The EIS measurements of CuNPs/μ-ES were recorded in 5 mM $K_3[Fe(CN)_6]$ and KCl (0.1 M) solution. An alternating potential with 10 mV amplitude was applied in the frequency range from 1 Hz to 10^6 Hz on microelectrode. All the potentials are reported with respect to the Ag/AgCl/Nafion™ electrode at an ambient temperature of 25 ± 2 ℃, unless otherwise stated.

3. Results and discussion

3.1. Surface characterization of microsensor

The X-ray photoelectron spectroscopy (XPS) and Raman spectroscopy studies of HD-CNT*f* have been reported in our recent study [69] confirming the absence of detectable metal catalyst and showed significant increment in D/G ratio for cross section compared to sidewall of HD-CNT*f*, respectively.

Raman spectroscopy on metal nanoparticles (NPs) substrate shows the enhancement in Raman intensity which is the result of localized surface plasmon resonance (LSPR). Silver (Ag), Gold (Au) and Copper (Cu) NPs are commonly used to study the surface enhanced Raman spectroscopy (SERS) sensors. The reason being Ag, Au, and Cu NPs exhibit LSPR in visible light due to excitation of the conduction electrons after interaction of light with matter [72–74]. Generally, the enhancement factor is expected to be 10^7–10^8 while few studies reported 10^{14}–10^{15} enhancement factor from single metal NP substrate [75]. Markin et al. reported that CuNPs possess a significant Raman enhancement (~10^5–10^7), which is comparable to Au and Ag NPs [76]. In this work, Raman spectroscopy was performed on bare HD-CNT*f* rod cross-section and CuNPs/HD-CNT*f* rod cross-section using 633 nm excitation wavelength irradiation. The different samples of CuNPs/HD-CNT*f* rod cross-section were prepared using controlled potential electrolysis (CPE) at different potentials i.e., −150, −250, −350 and −450 mV (FE-SEM shown in Fig. S3; Supporting Information).

In Fig. 2, the Raman spectra are shown for bare HD-CNT*f* rod cross-section (black curve) and different CuNPs/HD-CNT*f* samples. It can be seen that the Raman intensity of D, G and G′ band are enhanced for CuNPs/HD-CNT*f* as compared to bare HD-CNT*f* cross-section. The Raman relative intensities of the D, G and G′ peaks of bare HD-CNT*f* cross-section are about 1035, 1025 and 1130 counts, while the highest relative intensities of the D, G and G′ bands are observed 5835, 4800 and 4140 counts for CuNPs/HD-CNT*f* fabricated at −150 mV, which could be explained by the electric field enhancement induced by localized surface plasmon resonance [77]. At −150 mV potential, very low concentration of CuNPs were deposited at HD-CNT*f* and the deposition of CuNPs at HD-CNT*f* cross-section surface increased with increasing the reduction potential from −150 mV to −450 mV, which can be seen in FE-SEM images of Fig. S3 (Supporting Information). The enhancement factor or surface plasmon resonance (SPR) is dependent on the size, shape and roughness of metal NPs [73]. Due to increasing number of CuNPs at −350 mV, the CuNPs/HD-CNT*f* cross-section showed less intensity of D, G, and G′ band compared to CuNPs/HD-CNT*f* observed at −250 mV. At −450 mV, the CuNPs completely covered the HD-CNT*f* surface, and due to high packed density of CuNPs, the incident light is not able to interact with CNT surface and completely reflected from metal surface, which resulted to the negligible intensities of the D, G, and G′ band as shown in inset of Fig. 2. The enhancement factor for D peak is about 5.6 which is higher than G peak at CuNPs/HD-CNT*f*, since the enhancement in the D peak is caused by the CNTs cross-section defects and electromagnetic enhancement of CuNPs, while the G peak is merely caused by the electromagnetic enhancement of CuNPs [76].

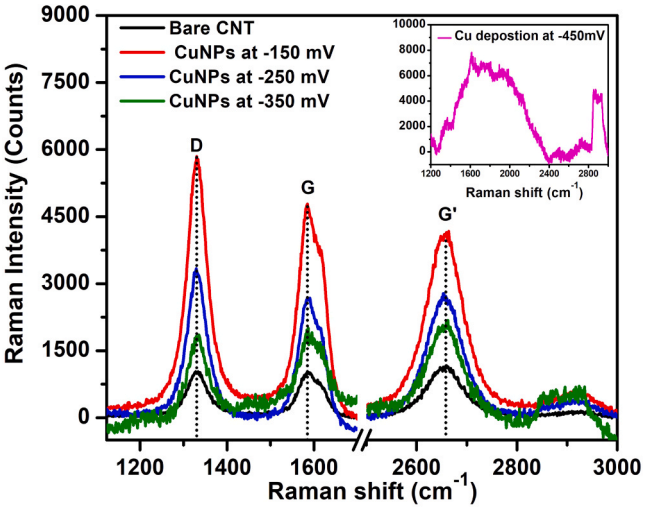

Fig. 2. Raman spectra of bare HD-CNT*f* cross-section and CuNPs/HD-CNT*f* cross-section. CuNPs were deposited at different constant potential i.e., −150, −250, and −350 using CPE. Inset shows the Raman spectrum of CuNPs deposited at −450 mV using CPE.

The Electrochemical impedance spectroscopy (EIS) was performed to analyze the charge transfer resistance of the bare and CuNPs modified HD-CNT*f* cross-section using Randles equivalent circuit. In high frequency region, the EIS results showed the impedance values 55k ohm and 20k ohm for bare and CuNPs/HD-CNT*f* surface, respectively as shown in Fig. 3. The reduction in charge transfer resistance for CuNPs modified CNT*f* cross-section can be attributed to CuNPs which increases the active surface area as compared to bare CNT*f* cross-section. An apparent difference is observed at low frequency, where the 45° sloped region of the Nyquist plots, the so-called Warburg resistance, can be seen for bare and CuNPs/HD-CNTf surface. The Warburg element typically is

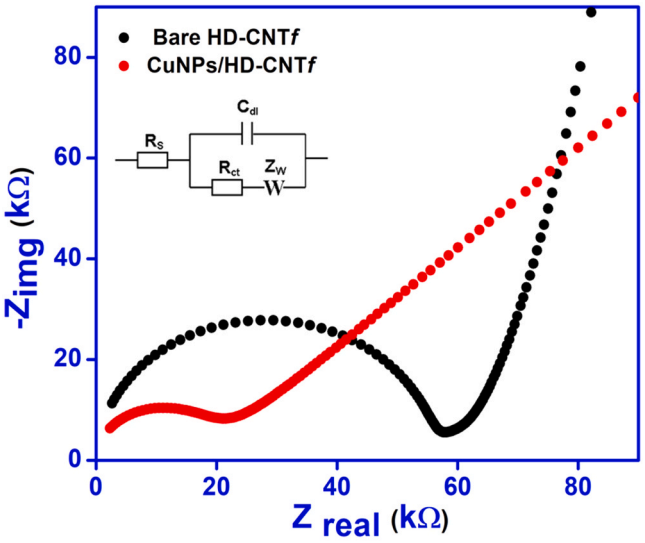

Fig. 3. Nyquist plots of bare and CuNPs modified HD-CNT*f* rods cross-section microelectrodes (inset is Randles equivalent circuit).

used to represent linear diffusion under semi-infinite conditions. The bare CNT*f* cross section surface has large number of oxygen functional groups due to the defects or open-ended sites (sp3 carbon) [59]. The high densification of CNTs with in fiber and presence of higher percentage of oxygen functional groups will hinder, to some extent, the transport of ions into pores which increases the Warburg impedance. The Warburg impedance slop approaches a vertical line with increasing the oxygen functional groups, which indicates an increase of ionic diffusion impedance in the pores [78]. The deposition of a porous CuNPs layer onto CNT*f* cross-section surface increases the ion diffusion and corresponding formation of the diffusion layer at electrode surface which leads to a straight line of Nyquist plot, which appears at 45° angle [78,79].

3.2. Cyclic voltammetric characterization

3.2.1. Ag/AgCl//Nafion™/HD-CNT*f* rod QRE

Initially, the fabricated Ag/AgCl/Nafion™ coated HD-CNT*f* rod electrode was examined as a quasi-reference electrode compared to the standard Ag/AgCl (3 M NaCl) commercial reference electrode. For examination, cyclic voltammograms were recorded in redox analyte i.e. 5 mM $[Ru(NH_3)_6]^{3+}$ and 50 mM KCl (1:1 ratio) at a scan rate of 100 mVs^{-1}, using μ-ES where bare HD-CNT*f* rods were used as working (~40 μm diameter) and counter electrode (~94 μm diameter). As shown in Fig. 4A, the redox potential of the voltammogram recorded using Ag/AgCl/Nafion™ coated HD-CNT*f* rod QRE shifted negatively by around ~100 mV compared to the commercial standard Ag/AgCl (3 M NaCl) RE. The difference in the redox potential attributed to the significant difference in the Cl^- ion concentration present in the internal filling solution (3 M NaCl) of commercial standard RE. Further, experiments were also performed with increased concentration of KCl supporting electrolyte solution but the redox potential of Ag/AgCl/Nafion™ coated HD-CNT*f* rod QRE was not affected (graph not shown), which can be the result of the Nafion coating (negatively charged) on Ag/AgCl nanoparticles which screened the Cl^- anions.

3.2.2. CuNPs/HD-CNT*f* rod WE

In order to confirm the impact of CuNPs modification on the HD-CNT*f* rod, further CVs were recorded on bare and CuNPs modified working electrode (~40 μm diameter) in 5 mM $[Ru(NH_3)_6]^{3+}$ and 50 mM KCl at a scan rate of 100 $mV{\cdot}s^{-1}$ using μ-ES where Ag/AgCl//Nafion™/HD-CNT*f* rods were used as QRE (~94 μm diameter) and bare HD-CNT*f* rods used as counter electrode (~94 μm diameter). A comparison of CVs at bare and CuNPs modified HD-CNT*f* rods is shown in Fig. 4B. The reduction peak current of $[Ru(NH_3)_6]^{3+}$ at CuNPs/HD-CNT*f* was found to increase by ~10.5 nA magnitude compared to the bare HD-CNT*f* which can be assigned to the increment in the surface area after CuNPs deposition at the cross section of HD-CNT*f* rod.

The effect of the scan rate (5–200 mVs^{-1}) on the CV behavior of bare μ-ES and CuNPs/μ-ES in redox analyte 5 mM $Ru(NH_3)_6]^{3+}$ and 50 mM KCl (1:1 ratio) was also investigated. The observed voltammetric measurements for the reduction of $[Ru(NH_3)_6^{3+/2+}]$ showed sigmoidal steady state cyclic voltammograms with a magnitude of several nanoamperes at lower scan rate (5 mVs^{-1}) (Fig. 5A and B) that is the characteristic of hemispherical diffusion at microelectrodes. For a disk-shaped microelectrode, the steady state i_{lim} value is given by the following Eq. (1):

$$i_{lim} = 4nFDaC \quad (1)$$

where n refers to the number of electrons transferred per redox event, *F* is the Faraday constant 96,485 C mol^{-1}, diffusion coefficient (*D*) of 8.2×10^{-6} cm^2 s^{-1} [80,81], radius (*a*) for the cross-section of 20 μm and *C* is the concentration 2.5 mM for $[Ru(NH_3)_6]Cl_3$. From Eq. (1), the calculated limiting current is ~16 nA, which is the same magnitude observed for the reduction of redox analyte at bare HD-CNT*f* cross-section (inset; Fig. 5A). In case of CuNPs/HD-CNT*f*, the observed limiting current is ~28 nA (inset; Fig. 5B) which is near to double of the limiting current observed at bare HD-CNT*f* cross section. The increment in the limiting current can be assigned to the deposition of CuNPs at the cross section of HD-CNT*f* which significantly increases the active surface area of the working microelectrode. Further increment in the scan rates (25–200 mVs^{-1}) shows small gentle peaks rather than steady-state current for both the forward and reverse scans. At higher scan rates the diffusion layer becomes smaller and mass transport is likely to have an increased contribution from planner diffusion. The CuNPs modified CNT*f* cross section (Fig. 5B) shows slightly higher capacitive background with hysteresis in the reverse scan but faradic current is also larger compared to bare CNT*f* cross section (Fig. 5A) which is due to increase in the surface area after CuNPs deposition. The observed hysteresis may be due to the adsorption of redox analyte decomposed product on CuNPs/HD-CNT*f* and its slight effect also can be seen in reverse scan where the oxidation peak cannot be defined as identical to the reduction peak, whereas bare CNT*f* cross section showed identical redox peak current for forward and reverse scan [69]. The ΔE_p values for bare and CuNPs modified HD-CNT*f* were calculated by using halfwave form as the observed redox response cannot be considered as transient. In such a condition, the half-peak potential is a convenient indicator to examine the charge transfer rates. The ΔE_p, for both bare HD-CNT*f* rod and CuNPs/HD-CNT*f* rod, is comparable with a difference in the 1/4-wave and 3/4-wave potential, $E_{1/4}$–$E_{3/4}$, in the range 55–59 mV, indicating reversible electrochemical reaction process with fast electron transfer kinetics at bare open ends and CuNPs modified HD-CNT*f* cross section.

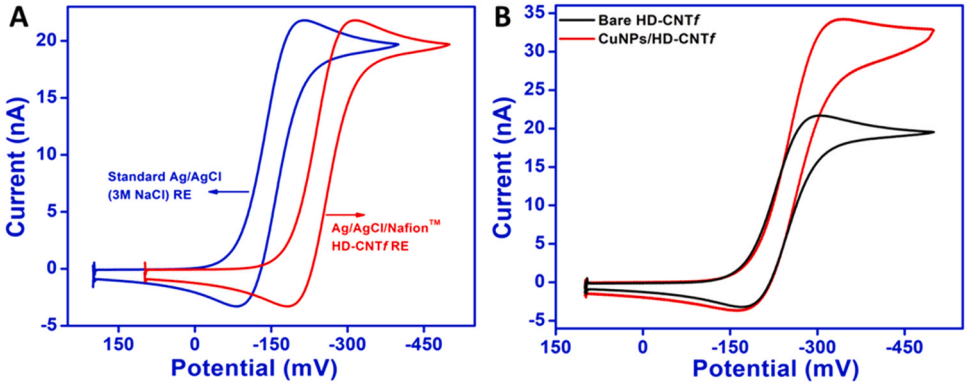

Fig. 4. CVs recorded in 5 mM $[Ru(NH_3)_6]^{3+}$ in 50 mM KCl (A) for a comparative evaluation of the commercial Ag/AgCl reference electrode (3 M NaCl) and Ag/AgCl/Nafion™/HD-CNT*f* rod quasi-reference electrode using bare HD-CNT*f* rod cross sections as the working and counter electrodes and (B) at bare and CuNPs/HD-CNT*f* rod working electrode using Ag/AgCl/Nafion™/HD-CNT*f* rod quasi-reference electrode and bare HD-CNT*f* rod counter electrode. Scan rate of 100 mVs^{-1}.

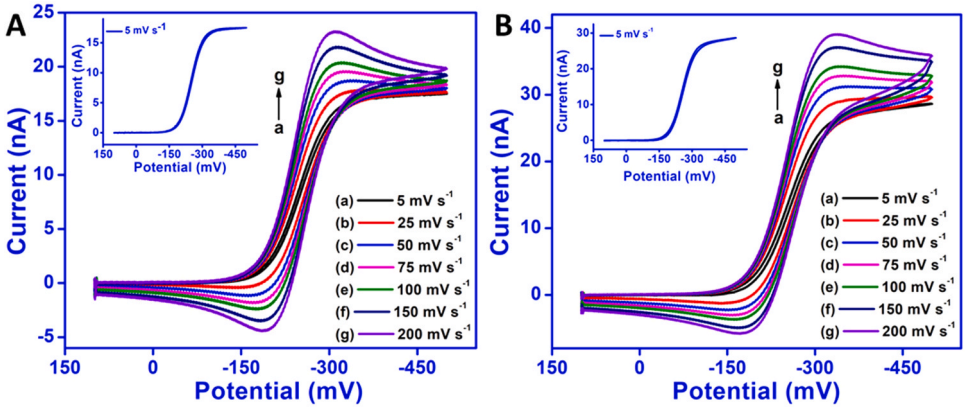

Fig. 5. Cyclic voltammetry of 5 mM $[Ru(NH_3)_6]^{3+}$ in 50 mM KCl with increasing scan rates in a range of 5–200 mV/s at (A) bare μ-ES and (B) CuNPs/μ-ES. Inset of both graphs show the CV recorded at a scan rate of 5 mV/s.

3.3. NaOH concentration optimization

The NaOH concentration is one of the key factors which affect the sensitivity of glucose oxidation on non-enzymatic electrode surfaces which can be explained by the formation of hydroxyl radicals at high potentials. Therefore, the effect of the NaOH concentration in the range of 10–500 mM on the current response for 0.5 M glucose was examined by CV at a scan rate of 50 mV·s^{-1}. In the absence of NaOH, no current response for glucose oxidation was observed. With the increase of NaOH concentration until 0.5 M NaOH, the peak potential shifts more positive. The anodic peak current for glucose oxidation was increased with a maximum current at 0.1 M NaOH and then decreased slowly upon increase of the NaOH concentration. Therefore, 0.1 M NaOH was selected as the supporting electrolyte for electrochemical experiments of glucose detection.

3.4. Electrooxidation of glucose on CuNPs/ HD-CNTf microsensor

Before implementing the CuNPs/HD-CNT*f* microsensor for glucose sensing, its electrochemical behavior was investigated in alkaline solution using CV. Fig. 6A shows successive cyclic voltammograms recorded on the CuNP-modified HD-CNT*f* microsensor in 0.1 M NaOH at a scan rate of 50 mV·s^{-1}. The current-potential curve became stable after six cycles (Fig. 6A) and seven peaks were observed, in good agreement with the electrochemical processes reported in the literature [82,83]. In the anodic wave, peak 1 was assigned to the adsorption of oxygen [84], whereas peak 2 was attributed to the transition of Cu(0)/Cu(I) (i.e., Cu_2O). Peak 3 was associated with the formation of Cu(II), which involves two transition processes (i.e., Cu(0)/Cu(II) and Cu(I)/Cu(II)). Peak 4 corresponded to the broad peaks observed in the first few scans that merged upon scanning and was due to the formation of soluble species (i.e., $HCuO^{2-}$) through the redox reactions of copper-based solid (s) and hydroxide ions [82]. Further anodic scanning above 250 mV (vs Ag/AgCl/Nafion™/HD-CNT*f*) led to the formation of Cu(III), which could only be detected at high hydroxide concentrations [83,84]. In the anodic potential region, the oxidation peak of Cu(II)/Cu(III) was not clearly observed. The formation of Cu(III) could be overlapped by the oxidative tail of water-splitting, observed as an increase in the current at 350–600 mV. In the cathodic scan, one small (peak 5) and two large reduction peaks (peaks 6 and 7) were observed, which were assigned to the conversion of Cu(III)/Cu(II), Cu(II)/Cu(I), and Cu(I)/Cu(0), respectively.

Fig. 6B displays the cyclic voltammograms obtained for the CuNPs/ HD-CNT*f* microsensor in the absence and presence of glucose in 0.1 M NaOH recorded at 50 mV·s^{-1}. Some notable differences were observed between the cyclic voltammograms obtained in the presence and absence of glucose. First, oxidation peak 2 for the formation of Cu(0)/Cu (I) was identical in the absence and presence of glucose, which indicates that there was no interaction between glucose and Cu(0) [82]. Second, peak 3, which corresponds to two transition processes (i.e., Cu(0)/Cu(II) and Cu(I)/Cu(II)) showed a sharp decrease in peak current in the presence of glucose, indicating a transition majorly from Cu(0) to Cu(II) due to the formation of a Cu(I)-glucose complex [82]. Third, the absence of peak 4 in the presence of glucose resulted from the absorption of glucose on the electrode catalytic sites, which prevented the further formation of soluble species by blocking the interactions between Cu-based solid(s) and hydroxide ions. Fourth, the dramatic increase in the anodic current signal at 230–500 mV in the presence of glucose indicated the

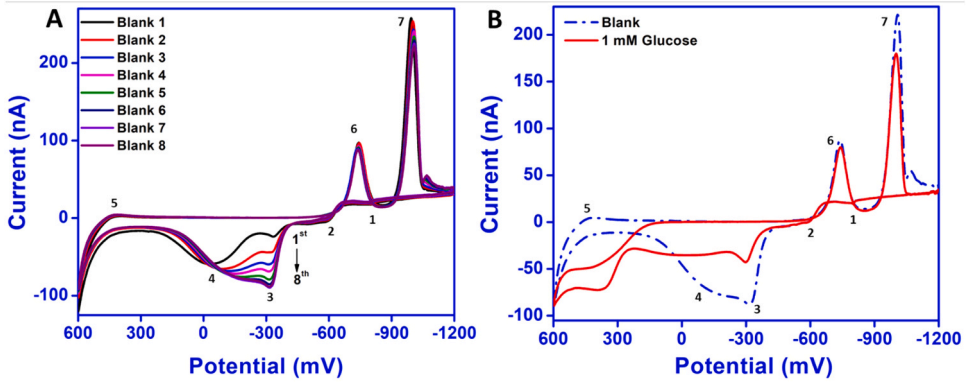

Fig. 6. (A) Consecutive cyclic voltammograms recorded on the CuNPs/ HD-CNT*f* microsensor in 0.1 M NaOH solution. (B) Cyclic voltammograms recorded on the CuNPs/ HD-CNT*f* microsensor in the absence (dotted line) and presence (solid line) of 1 mM glucose in 0.1 M NaOH. Scan rate of 50 mV·s^{-1}.

desorption of glucose from Cu(I) and the instantaneous electrocatalytic oxidation of glucose, which likely involved Cu(III) and hydroxyl radicals [82,84]. Another study suggested that this anodic signal could also be attributable to a shift in peak 4 for the conversion of Cu(I)/Cu(II) [83]. Fifth, in the cathodic scan, the absence of peak 5 in the presence of glucose provided evidence for the consumption of Cu(III) during the electrooxidation of glucose. Finally, tiny decreases in the currents of peaks 6 and 7, which correspond to the conversion of Cu(II)/Cu(I) and Cu(I)/Cu(0), respectively, were attributed to the formation of a Cu(I)–glucose complex during the anodic scan, which affects the formation of Cu(II) [82].

Although an accurate mechanism for glucose electrooxidation on copper-based electrodes in alkaline media has not been firmly established, the most detailed and confirmed work has been reported by Marioli et al. [82]. According to this study, glucose oxidation is activated by the deprotonation of glucose and isomerization to its enediol form followed by the formation of an intermediate by complexation or chelation with the electrode surface and oxidation by Cu(I), Cu(II), and Cu (III). Among the oxidation states of copper hydroxides, the Cu(III) form plays a major role in glucose oxidation. The conversion of Cu(II)/Cu(III) occurs at 250–600 mV. Thus, the glucose oxidation current signal was observed in this potential range because this reaction was strongly catalyzed by Cu(III) species, which acted as the main electron transfer mediator [36]. This behavior was further confirmed by the absence of the Cu(III) reduction peak (peak 5, Fig. 6B) in the cathodic scan, as the Cu(III) species were consumed in the oxidation of glucose. The entire process for the electrooxidation of glucose on the CuNPs/HD-CNT*f* surface can be summarized as follows:

$$Cu + 2OH^- \rightarrow Cu(OH)_2 + 2e^- \quad (2)$$

$$Cu(OH)_2 \rightleftarrows CuO + H_2O \quad (3)$$

$$Cu(OH)_2 + OH^- \rightleftarrows CuOOH + H_2O + e^- \quad (4)$$

or

$$CuO + OH^- \rightarrow CuOOH + e^- \quad (5)$$

$$CuOOH + Glucose + e^- \rightarrow CuO + OH^- + Gluconolactone \quad (6)$$

$$Gluconolactone \xrightarrow{Hydrolysis} Gluconic\ acid \quad (7)$$

To investigate the applicability of the proposed CuNPs/ HD-CNT*f* microsensor for nonenzymatic glucose sensing, CV measurements were performed at various glucose concentrations in 0.1 M NaOH at a scan rate of 50 mV·s^{-1}. In this experiment, a potential range of −200 to +500 mV (vs Ag/AgCl/Nafion™/HD-CNT*f*) was used, which is suitable for the amperometric study of glucose. As shown in Fig. 7A, the oxidation peak current increased linearly as the glucose concentration increased from 10 μM to 1 mM. No anodic current was observed in the absence of glucose, as shown by the dotted line. The linear relationship between the peak current and glucose concentration can be expressed by the following equation:

$$i_p\ (nA) = 0.0586[C_{glucose}(10–1000\ \mu M)] - 0.3023\ (R^2 = 0.998) \quad (8)$$

where i_p is the peak current and $C_{glucose}$ is the concentration of glucose. The wide linear range observed in the CV experiment indicates that CuNPs/HD-CNT*f* microsensor has excellent electrocatalytic activity toward the direct oxidation of glucose.

To elucidate the nature of the electron transfer kinetics, the electrooxidation of 0.5 mM glucose in 0.1 M NaOH was investigated at different scan rates (5–200 mV·s^{-1}). As shown in Fig. 7B, the anodic peak current for the oxidation of glucose increased linearly with the increasing scan rate. Linear relationships were observed for both i_p vs scan rate (ν) and log i_p vs log ν, as represented by Eqs. (9) and (10), respectively:

$$i_p\ (nA) = (0{\cdot}0994 \pm 0.0012)(\nu\ (mV{\cdot}s^{-1})) + (0{\cdot}7795 \pm 0.1370)\ R^2 = 0.998 \quad (9)$$

$$\log i_p\ (nA) = (0{\cdot}7896 \pm 0.0266)(\log \nu\ (mV{\cdot}s^{-1})) - (0{\cdot}5438 \pm 0.0462)\ R^2 = 0.993 \quad (10)$$

The linearity of the i_p vs ν plot (inset, Fig. 7B) and the slope value of ~0.789 (> 0.5) for the log i_p vs log ν plot indicate that the oxidation of glucose on CuNPs/HD-CNT*f* was a surface-controlled process [85].

Further, the electrooxidation of glucose was studied in a phosphate buffer solution of pH 7.4. The glucose oxidation did not show significant electrocatalytic activity on the surface of CuNPs/HD-CNT*f* in the phosphate buffer solution as compared to the NaOH solution.

3.5. Amperometry study

3.5.1. Applied potential optimization

The applied potential had a significant influence on the sensitivity, selectivity, and stability of the amperometric current of the developed sensor, therefore experiments were performed to first optimize the applied potential for glucose oxidation on CuNPs/HD-CNT*f*. For potential optimization, the amperometric experiments were performed at various potentials ranging from +250 mV to +450 mV (vs. Ag/AgCl/Nafion™/HD-CNT*f*) with the stepwise addition of 20 μM glucose in 0.1 M NaOH solution under stirring.

Fig. 8 shows the observed amperometric response of the CuNPs/HD-CNT*f* and it can be seen when the potential was increased from +250 to +400 mV, the electrode produces steady state current with gradual increment upon every addition of glucose. However, the highest

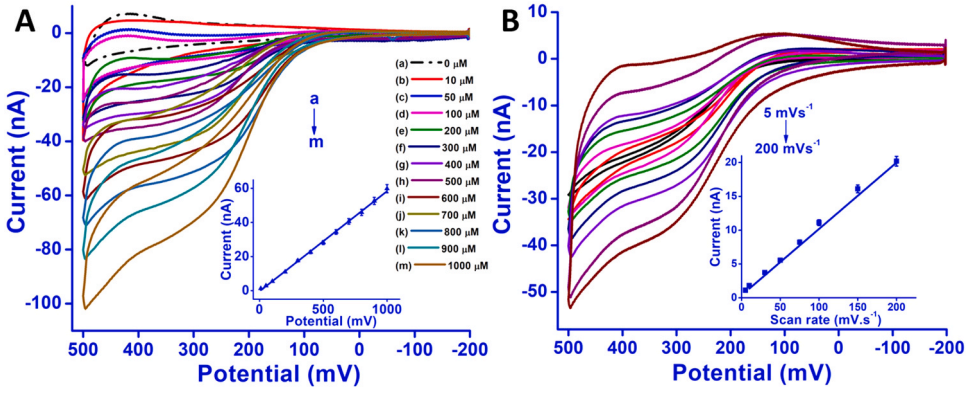

Fig. 7. (A) Cyclic voltammograms recorded on CuNPs/HD-CNT*f* microsensor in the presence of glucose at various concentrations: (a) 0, (b) 10, (c) 50, (d) 100, (e) 200, (f) 300, (g) 400, (h) 500, (i) 600, (j) 700, (k) 800, (l) 900, and (m) 1000 μM in 0.1 M NaOH at a scan rate of 50 mV·s^{-1}. (B) Cyclic voltammograms for 0.5 mM glucose recorded on the CuNPs/HD-CNT*f* microsensor in 0.1 M NaOH at scan rates of 5–200 mV·s^{-1}.

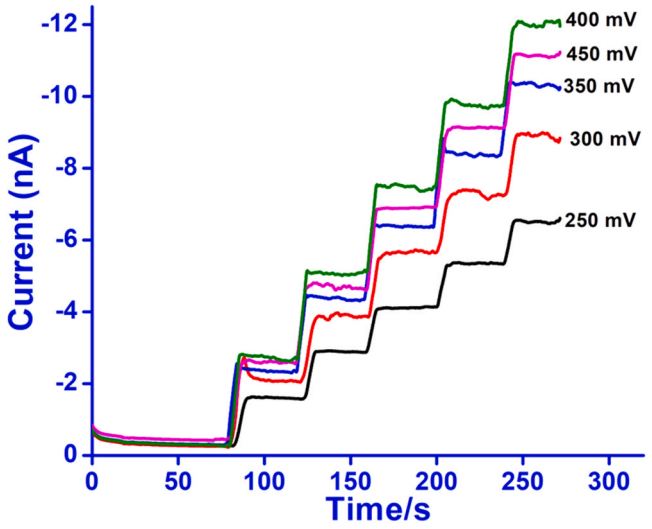

Fig. 8. Amperometric current responses of CuNPs/HD-CNT*f* at different potentials from +250 mV to +450 mV with successive addition of 20 μM glucose into 0.1 M NaOH solution.

oxidative current response was achieved at an applied potential of +400 mV and above that potential, current response was diminished, and one can see the significant difference between the current responses of 400 mV and 450 mV. This observation can be related to the probability of oxidation of other interfering species at higher applied potentials. Therefore, 400 mV was selected as an optimum applied potential for subsequent experiments.

3.5.2. *Amperometric detection of glucose*

The real-time amperometric detection of glucose on the CuNPs/HD-CNT*f* microsensor was carried out at a constant potential of +400 mV with the successive addition of various glucose concentrations (100 nM to 1 mM) into a stirred 0.1 M NaOH solution at 40 s intervals over multiple steps (Fig. 9A). After the addition of glucose, the current reached a steady state within 5 s, indicating that the microsensor had a fast electrocatalytic current response toward glucose electrooxidation. The observation of a significant current enhancement, even with the addition of only 0.1 μM glucose, confirmed the excellent electrocatalytic activity of CuNPs/HD-CNT*f*. As shown in Fig. 9B, the amperometric current response increased with increasing glucose concentration and the dependence of the oxidation current on the glucose concentration was found to have two linear ranges, which can be represented by Eqs. (11) and (12), respectively:

$$i_p\ (\text{nA}) = 0.076[C_{\text{glucose}}(0{\cdot}1\text{–}1450\ \mu\text{M})] + 0.992\ (R^2 = 0.997) \quad (11)$$

$$i_p\ (\text{nA}) = 0.040[C_{\text{glucose}}(1450\text{–}4450\ \mu\text{M})] + 58{\cdot}915\ (R^2 = 0.982) \quad (12)$$

where i_p is the current response and C_{glucose} is the glucose concentration in μM. The LOD was found to be 28 nM with a signal-to-noise ratio of 3. Based on the geometrical area of the electrode, the CuNPs/μ-ES displayed sensitivities of approximately 1942 and 1022 nA·μM^{-1}·cm^{-2} in the lower and higher concentration ranges, respectively. The decrease in sensitivity at higher concentrations can be attributed to intermediates formed during glucose electrooxidation being adsorbed on the electrode surface [35,36,65]. The CuNPs greatly enhanced the electrocatalytic activity and promoted electron transfer during glucose oxidation. Furthermore, the micrometer diameter and length of the highly densified well-aligned CNT*f* led to an increase in conductivity and a decrease in the non-faradic charging current compared to randomly dispersed carbon nanomaterials on macroelectrode surfaces or composites. This behavior was confirmed by the 30 pA current obtained after spiking with 100 nM glucose (inset, Fig. 9A), which is only observable at a microelectrode surface with an extremely low non-faradic charging current. The synergetic effect of electrocatalytic CuNPs and HD-CNT*f* provided a suitable detection limit, good sensitivity, and a rapid response time for glucose electrooxidation. The observed results showed that the proposed sensor has excellent electrocatalytic properties for nonenzymatic glucose sensing in minute sample volumes or even a single drop of testing fluid.

3.6. *Study of anti-interference and selectivity*

The enzymatic glucose determination relies on the oxygen which can be considered a major disadvantage. The oxygen limitation may result in the error of glucose quantification [6,7] Therefore, the anti-interference properties of the proposed CuNPs/HD-CNT*f* microsensor was examined against oxygen in 0.1 M NaOH solution at an applied potential of 400 mV. As can be seen in Fig. 10, neither the presence nor the removal of oxygen affects the glucose sensing performance. The observed results reveal the oxygen-independent behavior of proposed CuNPs/HD-CNT*f* based glucose microsensor.

One of the major concerns in nonenzymatic glucose sensing is the electrochemical oxidation signals from interfering species. The electroactive interfering species such as ascorbic acid (AA), dopamine (DA), uric acid (UA), other carbohydrate compounds such as fructose, lactose and sucrose and common ions like Na^+ and Cl^-, normally coexist with glucose in human blood, and can affect the glucose quantification. Another concern common with noble metal-based nonenzymatic glucose sensors is the poisoning by chloride ions, causing them to lose their sensing activity. The poisoning is caused by the coordination of Cl^- ions with metal/metallic oxides. Therefore, it is necessary to examine the electrochemical response of potential interfering species at CuNPs/

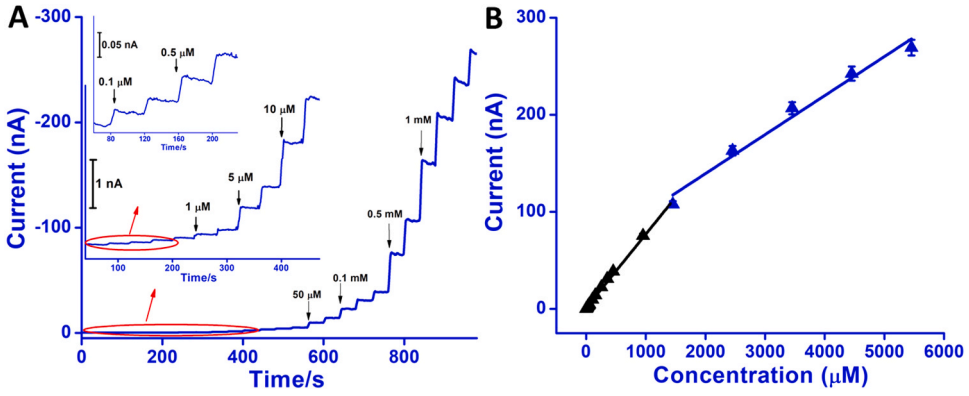

Fig. 9. (A) Amperometric response of CuNPs/HD-CNT*f* microsensor in 0.1 M NaOH solution to successive additions of glucose at concentrations from 100 nM to 1 mM at an applied voltage of 400 mV. (B) Corresponding calibration plot for the amperometric response of CuNPs/HD-CNT*f*.

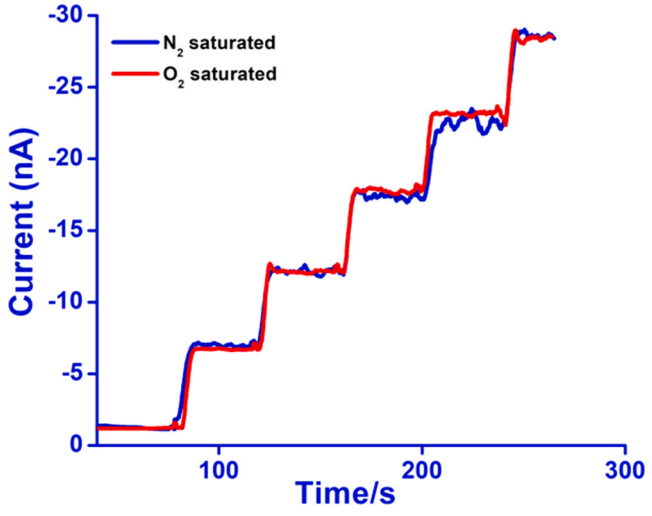

Fig. 10. Amperometric response of the CuNPs/ HD-CNT*f* to 50 μM glucose in air-saturated 0.1 M NaOH, (red graph) and nitrogen-purged 0.1 M NaOH (blue graph) at an applied potential of +400 mV. (For interpretation of the references to color in this figure legend, the reader is referred to the web version of this article.)

HD-CNT*f*. Considering the normal glucose concentration in human blood sample is at least 30 times higher than physiological interferences [35], the amperometric experiments were performed at +400 mV in stirred 0.1 M NaOH, by adding 100 μM glucose, followed with successive addition of 10 μM interfering species (AA, DA, UA, NaCl, and fructose, lactose, and sucrose). As shown in Fig. 11A, a well-defined current response was observed towards glucose addition, whereas the sensor shows insignificant response to the addition of AA, DA, UA and NaCl interfering species compared to the response from glucose, indicating the good selectivity of the sensor. This selectivity might be attributed to isoelectric point 9.5, CuO on the surface of CuNPs in 0.1 M NaOH solution (pH 12.5) would carry some negative charge (Cu-O$^-$) and negatively charged ions such as AA and UA would be repelled by partially negatively charged metal oxide layer, thus resulting in good selectivity. The AA, DA and UA concentrations are known to be less than 1/30 that of glucose in blood. Therefore, the proposed microsensor can be used to detect glucose in blood with negligible interference from AA, DA and UA. The interference from other co-existing carbohydrates i.e., lactose, sucrose and fructose also did not show any significant changes in current response, Fig. 11B. Considering the fact that the presence of commonly co-existing sugars in serum i.e., 8.1 μM for fructose [86] and 74 μM for sucrose [87] are significantly lower than glucose i.e. 4–7 mM in healthy human serum [88] and as both sugars would not introduce any significant signal in glucose detection, therefore, the blood sucrose and fructose is not anymore major concern for the proposed microsensor. Thus, it can be concluded that the CuNPs/μ-ES can be used for glucose detection in blood without being affected by potential interfering species.

3.7. Stability and reproducibility

To evaluate the stability of the proposed sensor, amperometric current response was recorded for stepwise addition of 0.2 mM glucose for 10 times in 0.1 M NaOH solution in a uniform time interval over a period of 15 days using five electrodes. The amperometric experiment was recorded daily up to 15 days and microsensors were stored under room temperature. The observed results reveal that the amperometric current response of glucose for all tested sensors remained unchanged for the first 7 days with relative standard deviation (RSD) under ± 2.6%. After 7 days, deviation in peak current with gradual variation or increase in RSD value was observed for all five electrodes. For repeatability, the amperometric current response was recoded for stepwise addition of 0.2 mM glucose concentration. The amperometric experiment was recorded repetitively five times on proposed microsensor at an interval of one hour. From the calculation, the observed RSD of the current response was ± 1.4%. Furthermore, the inter-electrode reproducibility was examined on five different microsensors under similar experimental conditions. The amperometric current response of glucose between five μ-ES varied only by a RSD of ± 2.2%. The observed results confirm that the proposed sensor has excellent stability and reproducibility and can be used for practical applications.

3.8. Real sample assays

To confirm the practical utility of the developed CuNP/μ-ES, glucose was determined in biological fluids (i.e., serum and urine samples). A 50 μL sample of serum was spiked into 25 mL of stirred 0.1 M NaOH solution and the current response was recorded at a constant potential of +400 mV. The observed amperogram showed a sharp increase in the amperometric peak current (Fig. 12A). Subsequently, this solution was spiked with a 50 μM standard glucose solution three times at 40 s intervals and the amperometric current response was recorded (Fig. 12A). The concentration of glucose in the spiked serum sample, as calculated using the calibration equation Eq. (11), was 9.31 μM, which agrees with the reported concentration in the serum sample (i.e., 4.55 mM, which gives a final concentration of 9.1 μM for 50 μL added to 25 mL NaOH solution). The measured concentrations of glucose in the spiked serum sample showed good reproducibility with a relative standard deviation (RSD) of ± 3% ($n = 3$). For exogenous spiking with a standard glucose solution at 10 μM, 50 μM and 100 μM concentrations, recovery values of

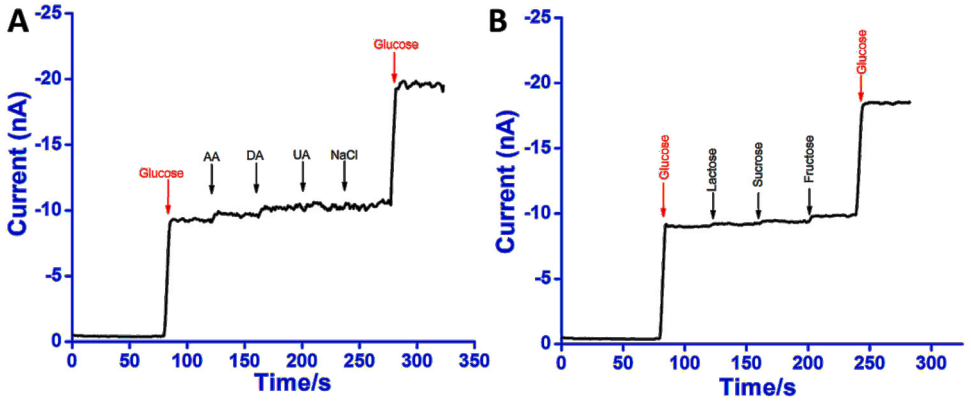

Fig. 11. Amperometric response of the CuNPs/ HD-CNT*f* to sequential injection of glucose (100 μM) and interfering species (A) 10 μM of AA, DA, UA, NaCl and (B) 10 μM lactose, sucrose and fructose in 0.1 M NaOH at an applied potential of +400 mV.

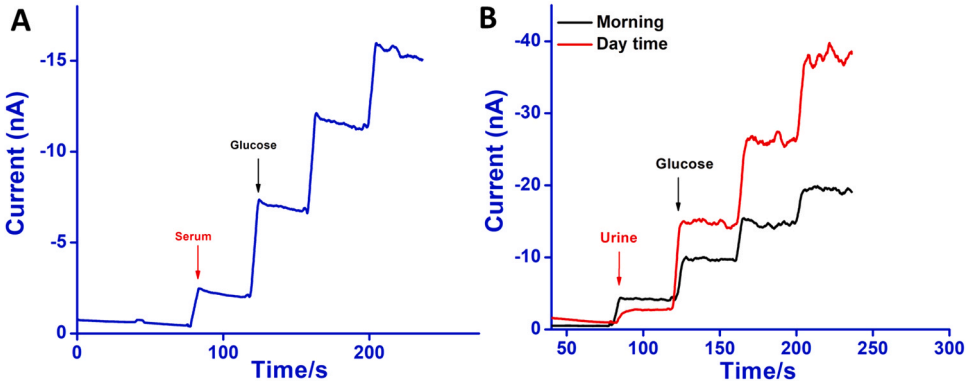

Fig. 12. Amperometric current responses of CuNPs/HD-CNT*f* microsensor in 0.1 M NaOH solution at 400 mV for initial injections of (A) serum with subsequent injections of 50 μM standard glucose solution and (B) urine sample with subsequent injections of 50 μM (Morning) and 100 μM (Day time) standard glucose solution.

102.36%, 99.3%, and 101.3% were obtained, respectively. Although the serum sample was reported to contain significant amounts of other compounds, including uric acid (205 μM), proteins (albumin and globulin, 305.55 mM), sodium (146 mM), potassium (4 mM), chloride (101 mM), calcium (0.34 mM), and phosphorus (0.20 mM), no interference with the glucose oxidation peak current was observed.

Further, the applicability of developed microsensor for the analysis of diabetic patient urine samples was evaluated. The urine samples were collected in the early morning and in the afternoon. The afternoon urine sample was collected 3 h after measuring the blood glucose concentration (208 mg/dL, as measured using Dexcom G6). At a constant potential of +400 mV, 50 μL of urine sample was spiked into 25 mL of stirred 0.1 M NaOH solution, followed by the addition of a 50 μM and 100 μM standard glucose solution in morning and daytime urine samples, respectively. As shown by the amperograms in Fig. 12B, the peak current for glucose oxidation was higher in the early morning urine sample than in the afternoon urine sample, which might be due to the overnight accumulation of glucose in urine. The glucose concentrations in the urine samples, as calculated using the calibration equation, were 5.8 and 17.43 mM in the afternoon and early morning urine samples, respectively. The glucose recovery was in the range of 97.92–101.60% with an RSD of ± 3%. The high accuracy and precision of the recovery results confirmed the reliability of the proposed CuNP/μ-ES for nonenzymatic glucose sensing in human biological samples.

4. Conclusion

In summary, a μ-ES was modified and employed for glucose detection. The μ-ES has three electrodes consisting of HD-CNT*f* cross-sections (~40 μm length), namely, a CuNP-deposited CNT*f* cross-section WE, a Ag/AgCl/Nafion™-coated CNT*f* cross-section QRE, and a bare CNT*f* cross-section CE. The μ-ES showed fast electron transfer kinetics in a redox analyte and the Ag/AgCl/Nafion™-coated CNT*f* QRE provided a sufficiently stable potential. The CuNP-deposited HD-CNT*f* WE showed excellent catalytic activity toward the electrooxidation of glucose in aqueous NaOH solution. The applicability of the developed CuNPs/HD-CNT*f* microsensor to nonenzymatic glucose detection was examined by CV and real-time amperometric measurements. These measurements revealed that the microsensor exhibits a low detection limit, wide quantification range, good precision, excellent selectivity, and a rapid response time. The performance of this microsensor can be attributed to the synergetic effect of electrocatalytic CuNPs and well-aligned HD-CNT*f*, which increases the conductivity with an extremely low non-faradic charging current. The developed microsensor was also free from chloride poisoning and the current response was independent of the oxygen concentration. Finally, the reported microsensor showed good accuracy and high precision for the analysis of healthy human serum and diabetic patient urine samples. Thus, the developed nonenzymatic CuNPs/μ-ES is suitable for the routine analysis of glucose in human biofluids, potentially even for single-droplet samples. The developed μ-ES, which can be used multiple times, also represents an advancement toward the development of microelectrode arrays using nonconventional and less-expensive techniques than lithography.

Supporting information

Schematic of CuNPs/μ-ES fabrication, EDX and FE-SEM of microsensor.

CRediT authorship contribution statement

Pankaj Gupta: Conceptualization, Methodology, Formal analysis, Investigation, Writing – original draft. **Vandna K. Gupta:** Methodology, Investigation. **Artur Huseinov:** Investigation, editing. **Connor E. Rahm:** Investigation, editing. **Kiera Gazica:** Investigation, editing. **Noe T. Alvarez:** Conceptualization, Resources, Writing – review & editing, Supervision, Project administration, Funding acquisition.

Declaration of Competing Interest

The authors declare that they have no known competing financial interests or personal relationships that could have appeared to influence the work reported in this paper.

Acknowledgments

The authors are indebted to professorship start-up funds from the Department of Chemistry at the University of Cincinnati, USA. NSF 2016484 PFI grant and Prof Shanov for providing the CNT fibers.

Notes

The authors declare no competing financial interest.

Appendix A. Supporting information

Supplementary data associated with this article can be found in the online version at doi:10.1016/j.snb.2021.130688.

References

[1] J.D. Newman, A.P.F. Turner, Home blood glucose biosensors: a commercial perspective, Biosens. Bioelectron. 20 (2005) 2435–2453, https://doi.org/10.1016/j.bios.2004.11.012.
[2] N. Quoc Dung, D. Patil, H. Jung, D. Kim, A high-performance nonenzymatic glucose sensor made of CuO–SWCNT nanocomposites, Biosens. Bioelectron. 42 (2013) 280–286, https://doi.org/10.1016/j.bios.2012.10.044.

[3] I.A. Macdonald, A review of recent evidence relating to sugars, insulin resistance and diabetes, Eur. J. Nutr. 55 (2016) 17–23, https://doi.org/10.1007/s00394-016-1340-8.

[4] M.H. Gabriel, D. Atkins, L. Chisholm, A. Noblin, Adverse events among patients with diabetes and ambulatory practice characteristics: evidence from a nationally representative survey, SAGE Open 8 (2018), 215824401878273, https://doi.org/10.1177/2158244018782732.

[5] M. García Lozano, Y. Peña García, J.A. Silva Gonzalez, C.V. Ochoa Bañuelos, M. P. Luevanos Escareño, N. Balagurusamy, Biosensors for Food Quality and Safety Monitoring: Fundamentals and Applications, in: Enzymes in Food Biotechnology, Elsevier, 2019, pp. 691–709, https://doi.org/10.1016/B978-0-12-813280-7.00040-2.

[6] H. Teymourian, A. Barfidokht, J. Wang, Electrochemical glucose sensors in diabetes management: an updated review (2010–2020), Chem. Soc. Rev. 49 (2020) 7671–7709, https://doi.org/10.1039/D0CS00304B.

[7] K.E. Toghill, R.G. Compton, Electrochemical non-enzymatic glucose sensors: a perspective and an evaluation, Int. J. Electrochem. Sci. 5 (2010) 1246–1301.

[8] P.-H. Hsiao, C.-Y. Chen, Insights for realizing ultrasensitive colorimetric detection of glucose based on carbon/silver core/shell nanodots, ACS Appl. Bio Mater. 2 (2019) 2528–2538, https://doi.org/10.1021/acsabm.9b00228.

[9] D. Lan, B. Li, Z. Zhang, Chemiluminescence flow biosensor for glucose based on gold nanoparticle-enhanced activities of glucose oxidase and horseradish peroxidase, Biosens. Bioelectron. 24 (2008) 934–938, https://doi.org/10.1016/j.bios.2008.07.064.

[10] X. Yang, Z. Zhou, D. Xiao, M.M.F. Choi, A fluorescent glucose biosensor based on immobilized glucose oxidase on bamboo inner shell membrane, Biosens. Bioelectron. 21 (2006) 1613–1620, https://doi.org/10.1016/j.bios.2005.08.004.

[11] J. Li, X. Li, R. Weng, T. Qiang, X. Wang, Penfluridol triggers mitochondrial-mediated apoptosis and suppresses glycolysis in colorectal cancer cells through down-regulating hexokinase-2, Anat. Rec. 304 (2021) 520–530, https://doi.org/10.1016/j.snb.2019.127349.

[12] D. Yang, S. Afroosheh, J.O. Lee, H. Cho, S. Kumar, R.H. Siddique, V. Narasimhan, Y.-Z. Yoon, A.T. Zayak, H. Choo, Glucose sensing using surface-enhanced raman-mode constraining, Anal. Chem. 90 (2018) 14269–14278, https://doi.org/10.1021/acs.analchem.8b03420.

[13] K.E. Shafer-Peltier, C.L. Haynes, M.R. Glucksberg, R.P. Van Duyne, Toward a glucose biosensor based on surface-enhanced Raman scattering, J. Am. Chem. Soc. 125 (2003) 588–593, https://doi.org/10.1021/ja028255v.

[14] L.E.A. Young, C.O. Brizzee, J.K.A. Macedo, R.D. Murphy, C.J. Contreras, A. A. DePaoli-Roach, P.J. Roach, M.S. Gentry, R.C. Sun, Accurate and sensitive quantitation of glucose and glucose phosphates derived from storage carbohydrates by mass spectrometry, Carbohydr. Polym. 230 (2020), 115651, https://doi.org/10.1016/j.carbpol.2019.115651.

[15] H. Wang, L. Hu, P. Zhou, L. Ouyang, B. Chen, Y. Li, Y. Chen, Y. Zhang, J. Zhou, Simultaneous determination of fructose, glucose and sucrose by solid phase extraction-liquid chromatography-tandem mass spectrometry and its application to source and adulteration analysis of sucrose in tea, J. Food Compos. Anal. 96 (2021), 103730, https://doi.org/10.1016/j.jfca.2020.103730.

[16] J. Wang, Glucose biosensors: 40 years of advances and challenges, Electroanalysis 13 (2001) 983–988, https://doi.org/10.1002/1521-4109(200108)13:12<983::AID-ELAN983>3.0.CO;2-%23.

[17] J. Wang, Electrochemical glucose biosensors, Chem. Rev. 108 (2008) 814–825, https://doi.org/10.1021/cr068123a.

[18] K. Tian, M. Prestgard, A. Tiwari, A review of recent advances in nonenzymatic glucose sensors, Mater. Sci. Eng. C 41 (2014) 100–118, https://doi.org/10.1016/j.msec.2014.04.013.

[19] D.W. Hwang, S. Lee, M. Seo, T.D. Chung, Recent advances in electrochemical non-enzymatic glucose sensors – a review, Anal. Chim. Acta 1033 (2018) 1–34, https://doi.org/10.1016/j.aca.2018.05.051.

[20] S. Park, S. Park, R.-A. Jeong, H. Boo, J. Park, H.C. Kim, T.D. Chung, Nonenzymatic continuous glucose monitoring in human whole blood using electrified nanoporous Pt, Biosens. Bioelectron. 31 (2012) 284–291, https://doi.org/10.1016/j.bios.2011.10.033.

[21] G. Chang, H. Shu, Q. Huang, M. Oyama, K. Ji, X. Liu, Y. He, Synthesis of highly dispersed Pt nanoclusters anchored graphene composites and their application for non-enzymatic glucose sensing, Electrochim. Acta 157 (2015) 149–157, https://doi.org/10.1016/j.electacta.2015.01.085.

[22] E. Sehit, J. Drzazgowska, D. Buchenau, C. Yesildag, M. Lensen, Z. Altintas, Ultrasensitive nonenzymatic electrochemical glucose sensor based on gold nanoparticles and molecularly imprinted polymers, Biosens. Bioelectron. 165 (2020), 112432, https://doi.org/10.1016/j.bios.2020.112432.

[23] S.-L. Zhong, J. Zhuang, D.-P. Yang, D. Tang, Eggshell membrane-templated synthesis of 3D hierarchical porous Au networks for electrochemical nonenzymatic glucose sensor, Biosens. Bioelectron. 96 (2017) 26–32, https://doi.org/10.1016/j.bios.2017.04.038.

[24] B. Zhu, L. Yu, S. Beikzadeh, S. Zhang, P. Zhang, L. Wang, J. Travas-Sejdic, Disposable and portable gold nanoparticles modified – laser-scribed graphene sensing strips for electrochemical, non-enzymatic detection of glucose, Electrochim. Acta 378 (2021), 138132, https://doi.org/10.1016/j.electacta.2021.138132.

[25] X. Chen, Z. Lin, D.-J. Chen, T. Jia, Z. Cai, X. Wang, X. Chen, G. Chen, M. Oyama, Nonenzymatic amperometric sensing of glucose by using palladium nanoparticles supported on functional carbon nanotubes, Biosens. Bioelectron. 25 (2010) 1803–1808, https://doi.org/10.1016/j.bios.2009.12.035.

[26] X. Xiao, G.A. Montaño, T.L. Edwards, C.M. Washburn, S.M. Brozik, D.R. Wheeler, D.B. Burckel, R. Polsky, Lithographically defined 3D nanoporous nonenzymatic glucose sensors, Biosens. Bioelectron. 26 (2011) 3641–3646, https://doi.org/10.1016/j.bios.2011.02.020.

[27] X. Chen, G. Li, G. Zhang, K. Hou, H. Pan, M. Du, Self-assembly of palladium nanoparticles on functional TiO2 nanotubes for a nonenzymatic glucose sensor, Mater. Sci. Eng. C 62 (2016) 323–328, https://doi.org/10.1016/j.msec.2016.01.068.

[28] J. Yang, X. Liang, L. Cui, H. Liu, J. Xie, W. Liu, A novel non-enzymatic glucose sensor based on Pt3Ru1 alloy nanoparticles with high density of surface defects, Biosens. Bioelectron. 80 (2016) 171–174, https://doi.org/10.1016/j.bios.2016.01.056.

[29] H. Jia, G. Chang, M. Lei, H. He, X. Liu, H. Shu, T. Xia, J. Su, Y. He, Platinum nanoparticles decorated dendrite-like gold nanostructure on glassy carbon electrodes for enhancing electrocatalysis performance to glucose oxidation, Appl. Surf. Sci. 384 (2016) 58–64, https://doi.org/10.1016/j.apsusc.2016.05.020.

[30] X. Bo, J. Bai, L. Yang, L. Guo, The nanocomposite of PtPd nanoparticles/onion-like mesoporous carbon vesicle for nonenzymatic amperometric sensing of glucose, Sens. Actuators B Chem. 157 (2011) 662–668, https://doi.org/10.1016/j.snb.2011.05.050.

[31] F. Xiao, F. Zhao, D. Mei, Z. Mo, B. Zeng, Nonenzymatic glucose sensor based on ultrasonic-electrodeposition of bimetallic PtM (M=Ru, Pd and Au) nanoparticles on carbon nanotubes–ionic liquid composite film, Biosens. Bioelectron. 24 (2009) 3481–3486, https://doi.org/10.1016/j.bios.2009.04.045.

[32] S. Nantaphol, T. Watanabe, N. Nomura, W. Siangproh, O. Chailapakul, Y. Einaga, Bimetallic Pt–Au nanocatalysts electrochemically deposited on boron-doped diamond electrodes for nonenzymatic glucose detection, Biosens. Bioelectron. 98 (2017) 76–82, https://doi.org/10.1016/j.bios.2017.06.034.

[33] N. Taşaltın, C. Taşaltın, S. Karakuş, A. Kilislioğlu, Cu core shell nanosphere based electrochemical non-enzymatic sensing of glucose, Inorg. Chem. Commun. 118 (2020), 107991, https://doi.org/10.1016/j.inoche.2020.107991.

[34] X. Niu, Y. Li, J. Tang, Y. Hu, H. Zhao, M. Lan, Electrochemical sensing interfaces with tunable porosity for nonenzymatic glucose detection: a Cu foam case, Biosens. Bioelectron. 51 (2014) 22–28, https://doi.org/10.1016/j.bios.2013.07.032.

[35] S. Shahrokhian, E. Khaki Sanati, H. Hosseini, Direct growth of metal-organic frameworks thin film arrays on glassy carbon electrode based on rapid conversion step mediated by copper clusters and hydroxide nanotubes for fabrication of a high performance non-enzymatic glucose sensing platform, Biosens. Bioelectron. 112 (2018) 100–107, https://doi.org/10.1016/j.bios.2018.04.039.

[36] Y. Zhang, L. Su, D. Manuzzi, H.V.E. de los Monteros, W. Jia, D. Huo, C. Hou, Y. Lei, Ultrasensitive and selective non-enzymatic glucose detection using copper nanowires, Biosens. Bioelectron. 31 (2012) 426–432, https://doi.org/10.1016/j.bios.2011.11.006.

[37] S.T. Farrell, C.B. Breslin, Oxidation and photo-induced oxidation of glucose at a polyaniline film modified by copper particles, Electrochim. Acta 49 (2004) 4497–4503, https://doi.org/10.1016/j.electacta.2004.05.007.

[38] Y. Zhao, J. Zhao, D. Ma, Y. Li, X. Hao, L. Li, C. Yu, L. Zhang, Y. Lu, Z. Wang, Synthesis, growth mechanism of different Cu nanostructures and their application for non-enzymatic glucose sensing, Colloids Surf. A Physicochem. Eng. Asp. 409 (2012) 105–111, https://doi.org/10.1016/j.colsurfa.2012.05.045.

[39] J. Zhao, L. Wei, C. Peng, Y. Su, Z. Yang, L. Zhang, H. Wei, Y. Zhang, A non-enzymatic glucose sensor based on the composite of cubic Cu nanoparticles and arc-synthesized multi-walled carbon nanotubes, Biosens. Bioelectron. 47 (2013) 86–91, https://doi.org/10.1016/j.bios.2013.02.032.

[40] D.-J. Chen, Y.-H. Lu, A.-J. Wang, J.-J. Feng, T.-T. Huo, W.-J. Dong, Facile synthesis of ultra-long Cu microdendrites for the electrochemical detection of glucose, J. Solid State Electrochem. 16 (2012) 1313–1321, https://doi.org/10.1007/s10008-011-1524-3.

[41] F. Sun, L. Li, P. Liu, Y. Lian, Nonenzymatic electrochemical glucose sensor based on novel copper film, Electroanalysis 23 (2011) 395–401, https://doi.org/10.1002/elan.201000391.

[42] S.K. Meher, G.R. Rao, Archetypal sandwich-structured CuO for high performance non-enzymatic sensing of glucose, Nanoscale 5 (2013) 2089–2099, https://doi.org/10.1039/c2nr33264g.

[43] C. Li, Y. Su, S. Zhang, X. Lv, H. Xia, Y. Wang, An improved sensitivity nonenzymatic glucose biosensor based on a CuxO modified electrode, Biosens. Bioelectron. 26 (2010) 903–907, https://doi.org/10.1016/j.bios.2010.07.007.

[44] H.-H. Fan, W.-L. Weng, C.-Y. Lee, C.-N. Liao, Electrochemical cycling-induced spiky Cu x O/Cu nanowire array for glucose sensing, ACS Omega 4 (2019) 12222–12229, https://doi.org/10.1021/acsomega.9b01730.

[45] H. Sim, J.-H. Kim, S.-K. Lee, M.-J. Song, D.-H. Yoon, D.-S. Lim, S.-I. Hong, High-sensitivity non-enzymatic glucose biosensor based on Cu(OH)2 nanoflower electrode covered with boron-doped nanocrystalline diamond layer, Thin Solid Films 520 (2012) 7219–7223, https://doi.org/10.1016/j.tsf.2012.08.011.

[46] S. Zhou, X. Feng, H. Shi, J. Chen, F. Zhang, W. Song, Direct growth of vertically aligned arrays of Cu(OH)2 nanotubes for the electrochemical sensing of glucose, Sens. Actuators B Chem. 177 (2013) 445–452, https://doi.org/10.1016/j.snb.2012.11.035.

[47] L. Bie, X. Luo, Q. He, D. He, Y. Liu, P. Jiang, Hierarchical Cu/Cu(OH)2 nanorod arrays grown on Cu foam as a high-performance 3D self-supported electrode for enzyme-free glucose sensing, RSC Adv. 6 (2016) 95740–95746, https://doi.org/10.1039/c6ra19576h.

[48] J. Liu, D. Xue, Rapid and scalable route to CuS biosensors: a microwave-assisted Cu-complex transformation into CuS nanotubes for ultrasensitive nonenzymatic glucose sensor, J. Mater. Chem. 21 (2011) 223–228, https://doi.org/10.1039/C0JM01714K.

[49] X. Zhang, G. Wang, A. Gu, Y. Wei, B. Fang, CuS nanotubes for ultrasensitive nonenzymatic glucose sensors, Chem. Commun. (2008) 5945–5947, https://doi.org/10.1039/b814725f.
[50] M. Cao, H. Wang, P. Kannan, S. Ji, X. Wang, Q. Zhao, V. Linkov, R. Wang, Highly efficient non-enzymatic glucose sensor based on CuxS hollow nanospheres, Appl. Surf. Sci. 492 (2019) 407–416, https://doi.org/10.1016/j.apsusc.2019.06.248.
[51] K.B. Male, S. Hrapovic, Y. Liu, D. Wang, J.H.T. Luong, Electrochemical detection of carbohydrates using copper nanoparticles and carbon nanotubes, Anal. Chim. Acta 516 (2004) 35–41, https://doi.org/10.1016/j.aca.2004.03.075.
[52] X. Kang, Z. Mai, X. Zou, P. Cai, J. Mo, A sensitive nonenzymatic glucose sensor in alkaline media with a copper nanocluster/multiwall carbon nanotube-modified glassy carbon electrode, Anal. Biochem. 363 (2007) 143–150, https://doi.org/10.1016/j.ab.2007.01.003.
[53] X. Li, Q. Zhu, S. Tong, W. Wang, W. Song, Self-assembled microstructure of carbon nanotubes for enzymeless glucose sensor, Sens. Actuators, B Chem. 136 (2009) 444–450, https://doi.org/10.1016/j.snb.2008.10.051.
[54] H.-X. Wu, W.-M. Cao, Y. Li, G. Liu, Y. Wen, H.-F. Yang, S.-P. Yang, In situ growth of copper nanoparticles on multiwalled carbon nanotubes and their application as non-enzymatic glucose sensor materials, Electrochim. Acta 55 (2010) 3734–3740, https://doi.org/10.1016/j.electacta.2010.02.017.
[55] T. Zhu, X. Wang, W. Chang, Y. Zhang, T. Maruyama, L. Luo, X. Zhao, Green fabrication of Cu/rGO decorated SWCNT buckypaper as a flexible electrode for glucose detection, Mater. Sci. Eng. C 120 (2021), 111757, https://doi.org/10.1016/j.msec.2020.111757.
[56] Y. Lin, F. Lu, Y. Tu, Z. Ren, Glucose biosensors based on carbon nanotube nanoelectrode ensembles, Nano Lett. 4 (2004) 191–195, https://doi.org/10.1021/nl0347233.
[57] Y. Tu, Y. Lin, Z.F. Ren, Nanoelectrode arrays based on low site density aligned carbon nanotubes, Nano Lett. 3 (2003) 107–109, https://doi.org/10.1021/nl025879q.
[58] J.J. Gooding, R. Wibowo, W. Liu, D. Yang, S. Losic, F.J. Orbons, J.G. Mearns, D. B. Shapter, Hibbert, Protein electrochemistry using aligned carbon nanotube arrays, J. Am. Chem. Soc. 125 (2003) 9006–9007, https://doi.org/10.1021/ja035722f.
[59] P. Gupta, K. Tsai, C.K. Ruhunage, V.K. Gupta, C.E. Rahm, D. Jiang, N.T. Alvarez, True picomolar neurotransmitter sensor based on open-ended carbon nanotubes, Anal. Chem. 92 (2020) 8536–8545, https://doi.org/10.1021/acs.analchem.0c01363.
[60] J. Wang, R.P. Deo, P. Poulin, M. Mangey, Carbon nanotube fiber microelectrodes, J. Am. Chem. Soc. 125 (2003) 14706–14707, https://doi.org/10.1021/ja037737j.
[61] D. Zhao, D. Siebold, N.T. Alvarez, V.N. Shanov, W.R. Heineman, Carbon nanotube thread electrochemical cell: detection of heavy metals, Anal. Chem. 89 (2017) 9654–9663, https://doi.org/10.1021/acs.analchem.6b04724.
[62] J. Yang, L.-C. Jiang, W.-D. Zhang, S. Gunasekaran, A highly sensitive non-enzymatic glucose sensor based on a simple two-step electrodeposition of cupric oxide (CuO) nanoparticles onto multi-walled carbon nanotube arrays, Talanta 82 (2010) 25–33, https://doi.org/10.1016/j.talanta.2010.03.047.
[63] J. Yang, W.-D. Zhang, S. Gunasekaran, An amperometric non-enzymatic glucose sensor by electrodepositing copper nanocubes onto vertically well-aligned multi-walled carbon nanotube arrays, Biosens. Bioelectron. 26 (2010) 279–284, https://doi.org/10.1016/j.bios.2010.06.014.
[64] F. Jiang, S. Wang, J. Lin, H. Jin, L. Zhang, S. Huang, J. Wang, Aligned SWCNT-copper oxide array as a nonenzymatic electrochemical probe of glucose, Electrochem. Commun. 13 (2011) 363–365, https://doi.org/10.1016/j.elecom.2011.01.026.
[65] L.-C. Jiang, W.-D. Zhang, A highly sensitive nonenzymatic glucose sensor based on CuO nanoparticles-modified carbon nanotube electrode, Biosens. Bioelectron. 25 (2010) 1402–1407, https://doi.org/10.1016/j.bios.2009.10.038.
[66] N.T. Alvarez, P. Miller, M.R. Haase, R. Lobo, R. Malik, V. Shanov, Tailoring physical properties of carbon nanotube threads during assembly, Carbon 144 (2019) 55–62, https://doi.org/10.1016/j.carbon.2018.11.036.
[67] N.T. Alvarez, P. Miller, M. Haase, N. Kienzle, L. Zhang, M.J. Schulz, V. Shanov, Carbon nanotube assembly at near-industrial natural-fiber spinning rates, Carbon 86 (2015) 350–357, https://doi.org/10.1016/j.carbon.2015.01.058.
[68] N.T. Alvarez, B. Ruff, M. Haase, R. Malik, N. Kienzle, D. Mast, M. Schulz, V. Shanov, Carbon nanotube fiber spinning, densification, doping and coating for microcable manufacturing, Recent Adv. Circuits, Commun. Signal Process. (2013) 336–341. ⟨http://www.sciencedirect.com/science/article/pii/S0257897213005094%0Ahttps://linkinghub.elsevier.com/retrieve/pii/S0257897213005094⟩.
[69] P. Gupta, R.A. Lazenby, C.E. Rahm, W.R. Heineman, E. Buschbeck, R.J. White, N. T. Alvarez, Electrochemistry of controlled diameter carbon nanotube fibers at the cross section and sidewall, ACS Appl. Energy Mater. 2 (2019) 8757–8766, https://doi.org/10.1021/acsaem.9b01723.
[70] P. Gupta, C.E. Rahm, B. Griesmer, N.T. Alvarez, Carbon nanotube microelectrode set: detection of biomolecules to heavy metals, Anal. Chem. 93 (2021) 7439–7448, https://doi.org/10.1021/acs.analchem.1c00360 (acs.analchem.1c00360).
[71] P. Hashemi, P.L. Walsh, T.S. Guillot, J. Gras-Najjar, P. Takmakov, F.T. Crews, R. M. Wightman, Chronically implanted, nafion-coated Ag/AgCl reference electrodes for neurochemical applications, ACS Chem. Neurosci. 2 (2011) 658–666, https://doi.org/10.1021/cn2000684.
[72] U. Kreibig, M. Vollmer, Optical Properties of Metal Clusters, Springer, Berlin, Heidelberg, 1995, https://doi.org/10.1007/978-3-662-09109-8.
[73] K.L. Kelly, E. Coronado, L.L. Zhao, G.C. Schatz, The optical properties of metal nanoparticles: the influence of size, shape, and dielectric environment, J. Phys. Chem. B 107 (2003) 668–677, https://doi.org/10.1021/jp026731y.
[74] J.A. Creighton, D.G. Eadon, Ultraviolet–visible absorption spectra of the colloidal metallic elements, J. Chem. Soc., Faraday Trans. 87 (1991) 3881–3891, https://doi.org/10.1039/FT9918703881.
[75] S. Nie, Probing single molecules and single nanoparticles by surface-enhanced Raman scattering, Science 275 (1997) 1102–1106, https://doi.org/10.1126/science.275.5303.1102.
[76] A.V. Markin, N.E. Markina, J. Popp, D. Cialla-May, Copper nanostructures for chemical analysis using surface-enhanced Raman spectroscopy, TrAC Trends Anal. Chem. 108 (2018) 247–259, https://doi.org/10.1016/j.trac.2018.09.004.
[77] X. Zhang, J. Zhang, J. Quan, N. Wang, Y. Zhu, Surface-enhanced Raman scattering activities of carbon nanotubes decorated with silver nanoparticles, Analyst 141 (2016) 5527–5534, https://doi.org/10.1039/C6AN00850J.
[78] Y. He, Y. Zhang, X. Li, Z. Lv, X. Wang, Z. Liu, X. Huang, Capacitive mechanism of oxygen functional groups on carbon surface in supercapacitors, Electrochim. Acta 282 (2018) 618–625, https://doi.org/10.1016/j.electacta.2018.06.103.
[79] M. Lenz, J. Zabel, M. Franzreb, New approach for investigating diffusion kinetics within capacitive deionization electrodes using electrochemical impedance spectroscopy, Front. Mater. 7 (2020) 1–12, https://doi.org/10.3389/fmats.2020.00229.
[80] Y. Wang, J.G. Limon-Petersen, R.G. Compton, Measurement of the diffusion coefficients of [Ru(NH3)6]3+ and [Ru(NH3)6]2+ in aqueous solution using microelectrode double potential step chronoamperometry, J. Electroanal. Chem. 652 (2011) 13–17, https://doi.org/10.1016/j.jelechem.2010.12.011.
[81] J.G. Limon-Petersen, J.T. Han, N.V. Rees, E.J.F. Dickinson, I. Streeter, R. G. Compton, Quantitative voltammetry in weakly supported media. Chronoamperometric studies on diverse one electron redox couples containing various charged species: dissecting diffusional and migrational contributions and assessing the breakdown of electroneutrality, J. Phys. Chem. C 114 (2010) 2227–2236, https://doi.org/10.1021/jp9097149.
[82] J.M. Marioli, T. Kuwana, Electrochemical characterization of carbohydrate oxidation at copper electrodes, Electrochim. Acta 37 (1992) 1187–1197, https://doi.org/10.1016/0013-4686(92)85055-P.
[83] P. Luo, S.V. Prabhu, R.P. Baldwin, Constant potential amperometric detection at a copper-based electrode: electrode formation and operation, Anal. Chem. 62 (1990) 752–755, https://doi.org/10.1021/ac00206a021.
[84] J.M.M. Droog, C.A. Alderliesten, P.T. Alderliesten, G.A. Bootsma, Initial stages of anodic oxidation of polycrystalline copper electrodes in alkaline solution, J. Electroanal. Chem. Interfacial Electrochem. 111 (1980) 61–70, https://doi.org/10.1016/S0022-0728(80)80075-1.
[85] M. Raj, P. Gupta, R.N. Goyal, Y.B. Shim, Graphene/conducting polymer nano-composite loaded screen printed carbon sensor for simultaneous determination of dopamine and 5-hydroxytryptamine, Sens. Actuators, B Chem. 239 (2017) 993–1002, https://doi.org/10.1016/j.snb.2016.08.083.
[86] T. Kawasaki, H. Akanuma, T. Yamanouchi, Increased fructose concentrations in blood and urine in patients with diabetes, Diabetes Care 25 (2002) 353–357, https://doi.org/10.2337/diacare.25.2.353.
[87] B. Vinet, B. Panzini, M. Boucher, J. Massicotte, Automated enzymatic assay for the determination of sucrose in serum and urine and its use as a marker of gastric damage, Clin. Chem. 44 (1998) 2369–2371, https://doi.org/10.1093/clinchem/44.11.2369.
[88] J.M. McMillin, Blood Glucose, third ed., Butterworth-Heinemann, Boston, 1990. https://www.ncbi.nlm.nih.gov/books/NBK248/.

Pankaj Gupta did his Masters in 2011 from Malaviya National Institute of Technology, Jaipur, and a Ph.D. in analytical chemistry from Indian Institute of Technology, Roorkee, India in 2017. Presently he is working as Postdoctoral Fellow of University of Cincinnati, USA. He is developing chemical and biosensors using carbon nanotubes.

Vandna K. Gupta is a postdoctoral researcher in the Department of Chemistry at the University of Cincinnati. She is working on the characterization of carbon nanotubes using spectroscopic techniques.

Artur Huseinov is a PhD student in the Department of Chemistry at the University of Cincinnati. His research is focused on development of electrochemical sensors.

Connor E. Rahm is a PhD student in the Department of Chemistry at the University of Cincinnati. His research is in the area of carbon nanotube printed electrochemical sensors.

Kiera Gazica is a PhD student in the Department of Chemistry at the University of Cincinnati. Her research is in the area of electrochemical sensors.

Noe T. Alvarez obtained Ph.D. in 2010 from Rice University, Houston TX. He is currently an assistant professor at University of Cincinnati, Cincinnati OH. Dr Alvarez is working on carbon nanotube synthesis and characterization, electroanalytical sensors and bio-materials development based on carbon nanotubes and graphene.